POLITECNICO
MILANO 1863

SCUOLA DI INGEGNERIA INDUSTRIALE
E DELL'INFORMAZIONE

EXECUTIVE SUMMARY OF THE THESIS

A fundamental analysis of transport properties of gas diffusion layers in CO_2 electroreduction

TESI MAGISTRALE IN CHEMICAL ENGINEERING – INGEGNERIA CHIMICA

AUTHOR: DAVIDE CAVUTO

ADVISOR: MATTEO MAESTRI

ACADEMIC YEAR: 2022-2023

1. Introduction

The intensive exploitation of non renewable natural resources has prompted the scientific community to seek sustainable alternative to fossils. In the industrial sector, particularly in chemical engineering, there is a growing focus on technologies capable of producing fuels and chemicals while minimizing their carbon footprint. CO2 electroreduction is an example of such a technology, as it enables carbon utilization for both direct air capture and industrial point source emissions. In a CO_2 electrolyzer the carbon dioxide is reduced to useful chemicals as carbon monoxide, methane, methanol, ethylene using renewable electricity. This "artificial photosynthesis" can be conducted in different reactor configurations. Among these, the vapor-fed CO_2 electrolyzer, in which carbon dioxide is directly fed as a gas stream, has proven superior performances compared to older technologies. With vapor-fed CO_2 electrolyzers, the production rate has been shown to be at least one order of magnitude higher compared to the previous configurations, paving the way for its industrial adoption. Despite these improvements, there are still many challenges preventing vapor-fed CO_2 electrolyzer to become a competitive industrial-scale technology. In Figure 1, it is possible to see how in order to improve the selectivity and the energy efficiency of the reactor the transport limitations need to be overcome by maximizing the CO_2 and electrons transport rate (red box). The present work aims to precisely address this challenge, by conducting a fundamental analysis of the gas diffusion layer (GDL), a porous media through which the CO_2 feed has to diffuse in order to reach the catalytically active sites of the reactor.

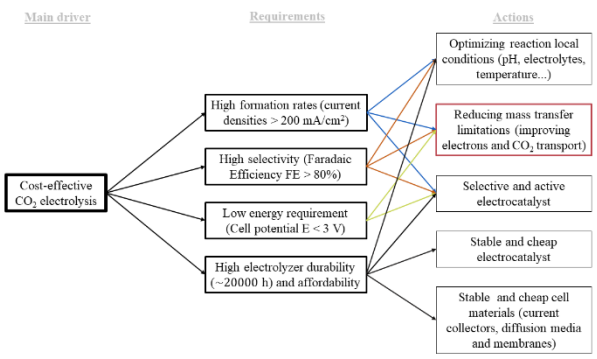

Figure 1 Current challenges in vapor-fed CO_2 electrolyzers for their economic sustainability.

2. Transport phenomena in gas diffusion electrodes

In Figure 2 a schematic representation of the cathodic chamber with a gas diffusion electrode is reported. The CO_2-rich gas is fed from the gas channel. Due to pressure and concentration driven flows, CO_2 is transported through the gas diffusion layer, made up of a macroporous layer and a microporous layer. On the microporous layer the catalyst particles are deposited forming the catalyst layer. The CO_2 is dissolved inside the electrolyte and after the diffusion towards the catalytic surface, it reacts to be reduced by the electrons provided by the water splitting in the anodic chamber. The electrons produced in the anode travel across an external circuit, through the gas diffusion layer, to the catalytic particles. It is clear that since the GDL regulates the flow of electrons and reactant/product species, its structure plays a pivotal role in determining the overall process efficiency.

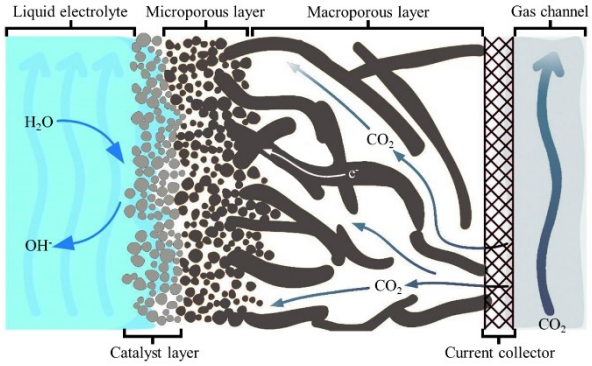

Figure 2 Gas diffusion electrode for CO_2 electroreduction structure. The CO_2 and the electrons are transported through the GDL to reach the catalytically active sites. Adapted from [1].

Indeed, particularly when the system is operating under high reaction rates, the CO_2 flux towards the active site has to rapidly replenish its surface concentration in order to avoid its depletion. At the same time, the porous gas diffusion media provides an ohmic resistance to the electron transport thus reducing the energy efficiency of the cell. In this sense, the simultaneous optimization of the transport phenomena occurring inside the GDL, requires a fundamental analysis of its structure-dependent transport properties. In this work, the effective solid conductivity, regulating the electrons and heat transport and the effective gaseous diffusivity, regulating the species diffusion, have been analyzed by the means of 3D numerical simulations carried out on virtual reconstructions of the GDL macroporous layer.

3. State of the art and motivation

A thorough literature analysis reveals the three main approaches which are utilized for investigating the effective transport properties of GDLs. The first method concerns experimental tests conducted on commercially available GDL while the remaining two methods employ numerical simulations carried out on virtual geometries. Virtual geometries can be obtained either by using micro-tomography scans (μCT) of GDL samples or by employing stochastic reconstruction methods. While the experimental and the tomography routes are limited by the commercial availability of physical samples to be analyzed, whose structural properties are fixed and seldom vary. On the contrary, if correctly validated, using stochastic reconstructions for building the GDL starting from its elementary building blocks (say carbon fibers), paves the way for systematically analyze the effect of microstructural parameters on the transport properties. The first efforts towards the implementation of this approach were pioneered by Schulz et al. [2], whose work tried to replicate the GDL structure by randomly placing an ensemble of straight cylinders in a finite volume. The physical GDL though, has more than one solid phase within it (Figure 3). The polyacrylonitrile (PAN) fibers are held together by a carbonaceous binder (typically a phenolic resin). Optionally, a hydrophobic material (PTFE, commonly known as Teflon) coats the GDL to increase its hydrophobicity [3]. As a result, subsequent studies have added to the carbon fiber structure the binder material and the PTFE to increase the representativeness of the GDL and improve the accuracy in the determination of the effective transport properties. Notably, the idea of using image processing techniques to add the binder material can be traced back to the work of Becker et al. [4]. Other successive studies have provided valuable insights but, to the knowledge of the author, a fundamental analysis on how the

microstructural features of GDLs are linked to their resulting effective transport properties is missing. Particularly, when deriving correlations for the effective conductivity and effective diffusivity, the porosity is assumed as a unique factor governing the transport. Nevertheless, before coming to such a conclusion the effect of relevant microstructural parameters needs to be assessed. In other words, a thorough parametric analysis of the effective transport properties in a wide range of void fraction and geometrical properties is required. To accomplish this goal, the microstructural parameters of the virtual GDL are systematically varied and the resulting effective transport property correlations are extracted by the means of CFD simulations.

As an additional fact, state-of-the-art GDE macroscopic modeling for CO2 electroreduction still relies [1] on the Bruggeman correlation, a correlation for the effective properties of isotropic porous media derived with theoretical arguments. This work draws attention to the fact that the predictions of the above mentioned correlation consistently deviate from both the derived and literature correlations, and as such are not suitable for describing the transport phenomena in macroscopic models of GDEs.

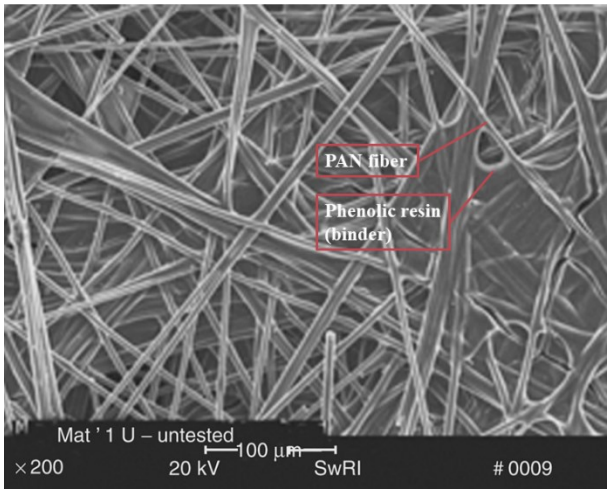

Figure 4 Carbon paper gas diffusion layer. The fibers are held together thanks to the binder, which alters the morphology of the GDL. Adapted from [3].

4. Methods

This work has been subdivided in three milestones as shown in Figure 3.

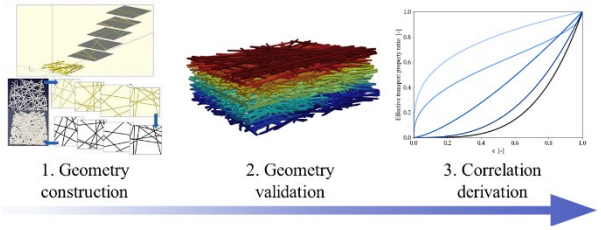

Figure 3 Milestones of the current work. After the geometry construction and validation, the correlation for the effective transport properties are derived.

4.1. Geometry construction

The geometry construction procedure can be conveniently subdivided in two steps:

1) PAN fiber (or skeleton) generation;
2) Binder addition.

An optimization loop is required in both the steps, in order to match the target porosity of commercial samples. The algorithmic procedure starts with the skeleton generation.

A fixed number of fibers (assumed to be perfectly straight cylinders) are randomly placed in the x-y plane to form a fiber layer. Next, several such fiber layers are stacked one over the other (allowing for a finite interpenetration of the layers) to create the complete carbon paper skeleton. The so-generated geometry is imported in the image processing software Fiji ImageJ as a 3D stack of 2D images (obtained by slicing the 3D skeleton). In ImageJ, the porosity of the skeleton is measured and compared to its desired value. If the porosity does not match, then the generation of the skeleton restarts, and, the number of fibers per layer is adjusted to reach the desired porosity in an optimization loop.

Once the skeleton is produced, morphological image processing is used to add the binder material. In particular, the closing operation (consisting in the subsequent Minkowski addition and subtraction) has the capability of replicating the wetting nature of the binder, that typically is accumulated at the fiber intersection, and therefore is chosen to add the binder. If the final porosity of the binder-added sample matches the desired value the procedure is finished and the image stack is converted in a stereolithography (stl) file. The geometry was constructed using OpenSCAD and ImageJ, whereas the entire optimization framework with this toolchain was implemented in Python.

The typical morphological information provided in the literature are the porosity of the sample ε and the binder volume fraction (BVF). Since for the skeleton generation its porosity is required, from the definition of the BVF it can be obtained that:

$$\varepsilon_{skeleton} = BVF\left(1-\varepsilon\right)+\varepsilon \qquad (1)$$

which constitutes the link between the porosity of the skeleton and the GDL sample porosity (please check the full manuscript for a more detailed explanation and a graphical visualization of the process).

4.2. Geometry validation

The generated virtual GDLs are validated by the means of two consecutive validation procedures:

1) Morphology validation;
2) Transport property validation.

In the morphology validation, the aim is to measure the extent to which the generation method is capable of mimicking the morphological features of the physical sample. In this work, the morphological features chosen for the analysis are the sectional porosity plots and the pore size distribution. The procedure to obtain the sectional porosity of the replicated samples is rather simple and it consists in calculating the porosity of each image of the 3D image stack and plotting the porosity values against the chosen coordinate. The plot provides information on the altering regions where solid phase is present, needed for heat and electricity conduction, and regions where void space is available for species to diffuse. The pore size distribution instead is obtained by simulating a Mercury Intrusion Porosimetry (MIP). While the experimental MIP is based on the penetration of liquid mercury inside the porous media due to an applied external pressure, the simulated MIP is not based on the physics of capillary systems but it is achieved by image processing techniques. A visual of this process is provided in Figure 5, where it can be observed for a generic porous medium the gradual filling of the void regions. Each snapshot of the above figure shows an iteration of the filling procedure, achieved by fitting a mercury sphere of fixed diameter. Once the iteration is completed, the volume of intruded mercury is linked with the diameter and a point of the cumulative PSD curve is obtained. It is worth mentioning that, based on how a pore is defined as a geometrical entity, different methods for measuring the pore size distribution can be employed, each of which provides a different estimation of the cumulative PSD plot. Therefore, when comparing these metrics, we have ensured that the PSD retrieved from literature were obtained through the MIP experimental technique.

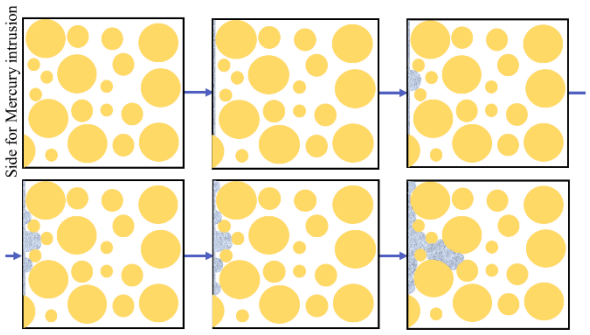

Figure 5 MIP simulation for a generic porous medium. From the left side of the geometry (selected for the intrusion) the algorithm will start to fit spheres of decreasing diameter, until all the void space gets filled.

The transport properties validation consists of conducting CFD simulations on the replicated geometries and computing the effective properties of the geometry in a selected direction. For calculating the effective transport properties the Laplace equation (Equation 2) has to be solved for the sought-after scalar fields (temperature or electric potential for solid conduction and concentration for the gas diffusion).

$$\nabla^2\phi = 0 \qquad (2)$$

The PDE is solved in OpenFOAM, using the laplacianFoam solver. A gradient of the selected scalar field ϕ is applied across the two opposing faces perpendicular to the specified flux direction (Dirichlet boundary condition) while on the remaining lateral walls the condition of zero flux is set (Neumann boundary condition). A second order discretization scheme is employed for the Laplacian operator and the simulations were assumed to be converged when the calculated residual is below 10^{-12}. The mesh independence study provided that a ratio of 4 between the fiber diameter and the grid size of the background mesh was enough to abate the discretization error. Moreover, the selected size of the computational

domain for the simulations was above the representative elementary volume (REV), meaning that it was ensured a solution independent from the size of the domain itself. Once the scalar field is known, the effective transport properties are calculated according to the effective porous media approximation as in Equation 3.

$$k_{eff} = \frac{L\int_{A^*} \boldsymbol{J} \cdot d\boldsymbol{A}^*}{A\left(\phi_1 - \phi_2\right)} \quad (3)$$

L being the distance among the two opposing faces where ϕ_1 and ϕ_2 are set as a Dirichlet BC. A is the cross-sectional area of these faces, and the numerator is the integral of the local flux (the information retrieved from the CFD simulation) times the local cross-sectional area. Please note that due to the anisotropicity of the GDL structure, for each transport property at least two values have to be determined, in the so called Through-plane (TP) and In-plane (IP) directions.

4.3. Correlations derivation

Once the validation step is complete, effective property correlations are developed by conducting parametric simulations for a set of GDL structural parameters. Four parameters are varied to assess their effect on the effective properties: porosity (ε), number of fibers per fiber layer (n), fiber diameter (d), binder volume fraction (BVF). The detailed explanation on the rationale behind the correlation development can be found in the complete manuscript.

5. Results

As seen in Figure 6, where a visual comparison of the virtual with the physical carbon paper is reported, the generation tool appears to be capable of generating realistic representations of the commercial GDLs once their structural parameters are provided. The comparison looks valid also in quantitative terms, as demonstrated by the sectional porosity plots and by the pore size distribution of selected physical GDLs (Figure 7 and Figure 8, respectively). The sectional porosity plots highlight a periodic trend in the porosity across the TP direction for both the virtual reconstruction and the experimentally obtained curves.

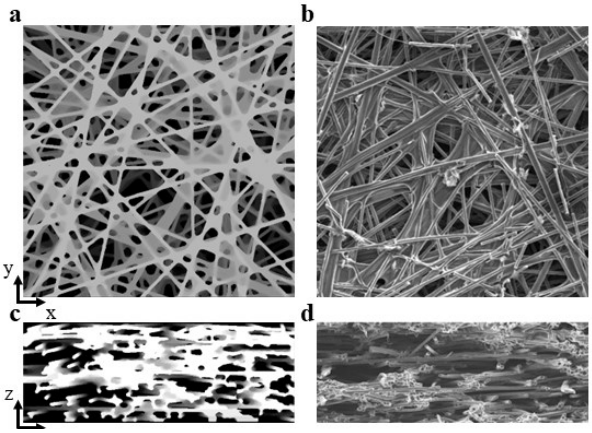

Figure 6 Visual comparison of the virtual and physical GDL samples. **a**, Virtual TP view. **b**, Physical TP view [5]. **c**, Virtual IP view. **d**, Physical IP view [5].

The difference between the two curves appears in the amplitude and the frequency of the oscillations. The oscillations are a direct consequence of the manufacturing process of carbon paper in which thin fiber sheets are compression molded to reach the desired thickness of the paper. In this sense the virtual geometry reconstruction captures, even if not precisely, the alternating regions of high and low voidage.

In Figure 8 instead, it is clear that although the experimental and simulated curves do not completely overlap, the former define a range (gray shaded area representing an experimental spread in the data) of cumulative PSD, within which the simulated PSD consistently fits. This observation is particularly significant considering that all the studied GDLs are identical commercial GDLs (Toray TGP-H).

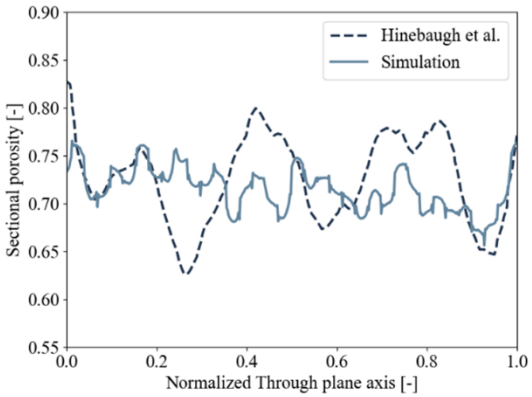

Figure 7 Sectional plot validation with selected literature μCT data. Commercial GDL analyzed:Toray TGP-H 90, ε = 0.74 [5].

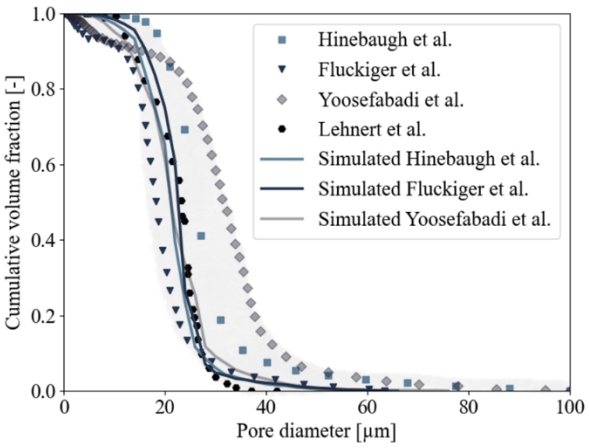

Figure 8 Cumulative PSD of selected GDLs. Experimentally measured curves (dotted lines, references in the full document) compared to MIP simulation of the virtual reconstructions (full lines).

Continuing with the transport properties validation, in Table 1 the results of the transport simulations performed on literature available GDLs samples are reported and compared with the results of experimental transport tests. Considering the range of variation reported in experimental measurements of effective diffusivity and effective conductivity (10-20 %), the computed values can be considered physically sound and in agreement with the experimentally observed properties.

Once the geometry has been correctly validated, a detailed simulation campaign was carried out to unravel the dependence of the effective transport properties on the selected microstructural parameters (n Fiber, Fiber diameter, ε and BVF).

Table 1 Validation of effective conductivity and effective diffusivity predicted by virtual GDL reconstructions. Legend in the appendix A.

	ε	Fiber diameter [μm]	BVF	STPC	LTPC	SIPC	LIPC	STPD	LTPD	SIPD	LIPD
Yoshimune et al*.	0.74	8	40%	-	-	-	-	0.3859	0.36±0.02	-	-
Yoosefabadi et al.	0.75	7	45%	0.0114	0.0162	0.1716	0.1587 - 0.1846 ‡	0.2794	0.26-0.32	0.5821	0.557-0.586 ‡
Becker et al.	0.74	7	50%	0.0140	0.0122	0.1466	0.142	0.2328	0.29	0.5781	0.51
Fluckiger et al.	0.78	8	30%	-	-	-	-	0.4481	0.37	0.5912	0.587
García-Salaberri et al.	0.75	8	40%	0.0140	0.0087 -0.022	0.1715	0.159-0.177	0.3945	0.28-0.34	0.5056	0.52-0.6

A detailed analysis has revealed that, with the exception of the through-plane effective diffusivity, all the effective transport properties can be described as a unique function of the porosity of the sample. In Figure 9, the data points obtained from the simulation campaign are compared with the effective transport properties predicted by correlations selected from literature, over the range of investigated porosities (from 0.68 to 0.8).

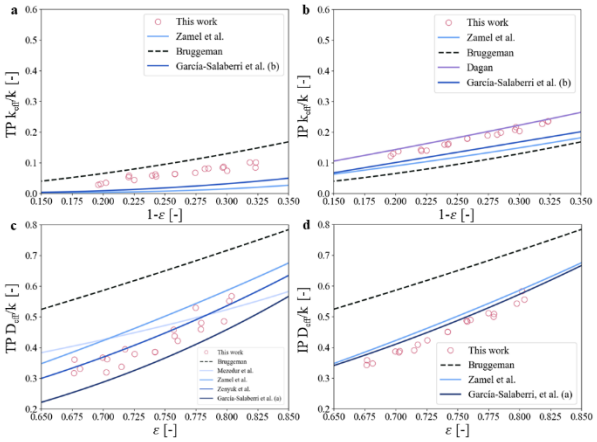

Figure 9 Calculated effective transport property ratios vs selected literature correlations. **a**, TP conductivity. **b**, IP conductivity. **c**, TP diffusivity. **d**, IP diffusivity. References in the full document.

The predicted effective diffusivity in both the TP and IP direction closely approaches the literature correlations curve, which further supports the possibility of relying solely on the porosity as a basis for the entire functional relationship. Concerning the effective conductivity, for which to the knowledge of the author also less correlations have been developed, a slightly higher discrepancy with the literature curves is reported. Apart from the Dagan correlation (which has been obtained from theoretical arguments for porous media) the CFD-simulation derived points consistently show an overprediction of the effective conductivity (in both the TP and IP directions). This may be due to the fact that in the current work the PAN fiber and binder resin have been assigned the same thermal conductivity while it is known that the binder has a slightly lower thermal conductivity. As an additional remark, it is possible to see how the Bruggeman correlation, typically used for GDE modeling, significantly overpredicts the effective diffusivity property when applied for gas diffusion layer. In terms of ε/τ models, this is equivalent to

say that the Bruggeman correlation predicts less tortuosity (τ) with respect to what the CFD simulations (and the previous literature results) predict. The effect is less pronounced for the effective conductivity for which a slight overestimation (underestimation) in the TP (IP) direction is obtained.

The distance between the curve fitted and the data points is minimized through a regression and the correlations obtained are reported in Figure 10 (for all the transport properties a power law has been used while for the IP conductivity using a linear equation has provided a better fit). From the figure it is evident that the anisotropicity of the geometry is particularly reflected in the effective conductivity, whose IP values are 2-4 times higher than the TP values. On the contrary, the anisotropy effect is somewhat negligible for the effective diffusivity, for which the IP value is slightly higher than the TP one. The latter result is not in accordance with previous literature findings that highlighted high anisotropicity also for the effective diffusivity, and as such will be subject of further investigations in future works.

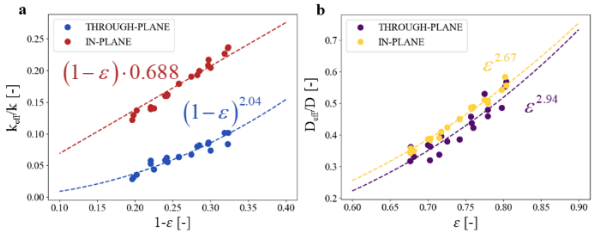

Figure 10 Correlations for GDL effective transport properties. **a**, Effective conductivity. **b**, Effective diffusivity.

6. Conclusions

In this work, the effective solid thermal conductivity and effective gaseous diffusivity of gas diffusion layers commonly employed in vapor-fed CO_2 electrolyzer, have been analyzed by means of 3D computational fluid dynamics simulations on virtually-generated GDL samples. The aim was to assess the dependence of the effective transport properties on structural microparameters such as the fiber diameter, the binder volume fraction, the number of fibers per fiber layer and the porosity. After having conducted a detailed simulation campaign, a negligible dependence for all the parameters except from the porosity has been found. Correlations for describing the effective properties of the GDL as a function of the porosity were determined and compared with empirically derived and theoretically based correlations for GDL porous media. The Bruggeman correlation, typically employed in the description of transport in porous media has been shown to be substantially inaccurate in the prediction of GDLs effective transport properties. Apart from the specific results achieved in the current work, from a methodological standpoint, this study presents a unified simulation framework to generate virtual electrode structures to replicate the overall characteristics of physical gas diffusion layers, simulating transport processes and hierarchically refining the macroscopic lumped parameters, facilitating the precise investigation of the effective transport properties. As such, the study is deemed to be insightful in enhancing the understanding of GDLs structure-dependent properties, a knowledge that is particularly useful when thinking of engineering the gas diffusion media of electrochemical cells.

References

[1] L.-C. Weng, A. T. Bell and A. Z. Weber, "Modeling gas-diffusion electrodes for CO2 reduction," *Phisycal Chemisty Chemical Physics*, vol. 20, pp. 16973-16984, 2018.

[2] V. P. Schulz, J. Becker, A. Wiegmann, P. P. Mukherjee and C.-Y. Wang, "Modeling of Two-Phase Behavior in the Gas Diffusion Medium of PEFCs via Full Morphology Approach," *Journal of The Electrochemical Society*, vol. 154, no. 4, pp. B419-B426, 2007.

[3] M. Mathias, J. Roth, J. Fleming and W. Lehnert, "Diffusion media materials and characterisation," in *Handbook of Fuel Cells – Fundamentals, Technology and Applications*, vol. 3, Wiley, 2003.

[4] J. Becker, R. Flückiger, M. Reum, F. N. Büchi, F. Marone and M. Stampanoni, "Determination of Material Properties of Gas Diffusion Layers: Experiments and Simulations Using Phase Contrast Tomographic Microscopy," *Journal of The Electrochemical Society*, vol. 156, no. 10, pp. B1175-B1181, 2009.

[5] J. Hinebaugh, J. Gostick and A. Bazylak, "Stochastic modeling of polymer electrolyte membrane fuel cell gas diffusion layers – Part

2: A comprehensive substrate model with pore size distribution and heterogeneity effects," *International Journal of Hydrogen Energy*, vol. 42, no. 24, pp. 15872-15886, 2017.

7. Appendix A

Table 1 legend

Symbol	Meaning
STPC	Simulation Through-Plane Conduction
LTPC	Literature Through-Plane Conduction
SIPC	Simulation In-Plane Conduction
LIPC	Literature In-Plane Conduction
STPD	Simulation Through-Plane Diffusion
LTPD	Literature Through-Plane Diffusion
SIPD	Simulation In-Plane Diffusion
LIPD	Literature In-Plane Diffusion
*	Fiber diameter and BVF assumed due to missing data
ǂ	Values from numerical models

For the references please check the complete manuscript.